Adsorption and Desorption Kinetics of n -Octane and n -Nonane Vapors on Activated Carbon

ARTICLE *in* LANGMUIR · SEPTEMBER 1999

Impact Factor: 4.46 · DOI: 10.1021/la9814992

2 AUTHORS:

Ashleigh Fletcher
University of Strathclyde
43 PUBLICATIONS **2,921** CITATIONS
SEE PROFILE

Keith Mark Thomas
Newcastle University
198 PUBLICATIONS **10,320** CITATIONS
SEE PROFILE

Adsorption and Desorption Kinetics of *n*-Octane and *n*-Nonane Vapors on Activated Carbon

Ashleigh J. Fletcher and K. Mark Thomas*

Northern Carbon Research Laboratories, Department of Chemistry, Bedson Building, University of Newcastle upon Tyne, Newcastle upon Tyne NE1 7RU, U.K.

Received October 26, 1998. In Final Form: May 26, 1999

This investigation has involved the study of the adsorption and desorption kinetics of two *n*-alkanes on a wood-based active carbon (BAX950). The adsorption and desorption characteristics of *n*-octane vapor on the activated carbon were investigated over the relative pressure (p/p^o) range 0−0.97 for temperatures in the range 288−313 K in a static vapor system. The adsorption characteristics of *n*-nonane were studied over the relative pressure range 0−0.97 and temperature range 303−323 K. The adsorption and desorption kinetics were studied with different amounts of preadsorbed *n*-octane for set changes in relative vapor pressure (p/p^o). The desorption kinetics were much slower than the corresponding adsorption kinetics for the same pressure step. The rate constants for adsorption increased with increasing relative pressure and surface coverage. The kinetic data for adsorption were used to calculate the activation energies for each increase in relative pressure. The activation energy was highest at low p/p^o and decreased with increasing p/p^o until a maximum was reached at $p/p^o \sim 0.075$. *n*-Nonane adsorption showed similar trends in adsorption kinetics and activation energies to the *n*-octane adsorption. The results are discussed in terms of diffusion in the pore structure in relation to the adsorption isotherm and mechanism.

1. Introduction

Carbons are widely used for the adsorption of environmentally unfriendly species from both gas and liquid phases.[1] This process is used in the final stages of emission abatement to remove the very low levels of pollutants that inevitably remain after removal of higher concentrations by other methods. Many pollutants requiring removal, especially from industrial plants and processes, are organic species and hydrocarbons.[2] One of the problems with this method is competitive adsorption with other species present in the process stream which may have a marked effect on the adsorption characteristics.

Activated carbons have hydrophobic sites comprising of the graphene basal plane layers and hydrophilic sites comprising of the functional groups (carbonyl, phenolic, lactone, etc.). The hydrophobic graphene layer surfaces act as primary adsorption sites for hydrocarbons while the hydrophilic functional groups act as the primary adsorption sites for water vapor. Previous investigations of the adsorption of *n*-octane vapor on carbon are limited.[3−5] The adsorption of *n*-nonane on activated carbons has been studied extensively in connection with its use as a preadsorption method to block micropores.[6,7] The kinetics are of critical importance in assessing the performance of active carbon beds for the adsorption of such species. However, there is much less information available on the adsorption kinetics of gases and vapors. Studies of the adsorption of gases on carbon molecular sieves (CMS) have shown that the adsorption kinetics follow a linear driving force (LDF), a combined barrier resistance/diffusion model or Fickian diffusion depending on the experimental conditions, porous structure, and the structural and electronic characteristics of the adsorptives.[8,9] The adsorption of water vapor on CMS and active carbons also follows an LDF mode.[10,11] However, the dependence of rate constant on amount adsorbed is complex. A barrier to diffusion into the carbon is produced by the development of water molecule clusters around the functional groups. It is apparent that the adsorption kinetics are a function of the adsorption mechanism.

The objective of the present study was the investigation of the adsorption characteristics of *n*-octane and *n*-nonane vapor on an activated carbon as a function of relative pressure and temperature. This study of the adsorption kinetics of pure vapors represents the initial part of a research program for studying the effect of changes in atmospheric conditions on organic vapor adsorption to understand the performance of activated carbons in filtering processes, in terms of pore structure, adsorption kinetics, and the adsorption mechanism.

2. Experimental Section

2.1. Materials Used. Carbon BAX950, a wood-based activated carbon, was obtained from the Westvaco Corporation, Virginia. The particle size fraction of the carbon was 1−2 mm. The *n*-octane and *n*-nonane used were both of 99% purity and were supplied by Aldrich Chemical Co., Inc, Milwaukee.

2.2. Static Atmosphere Adsorption Kinetics. The apparatus used was an intelligent gravimetric analyzer (IGA) supplied by Hiden Analytical, Ltd. This apparatus allows isotherms and the corresponding kinetics of adsorption and desorption, for set pressure steps, to be determined.[12] The balance

* To whom all correspondence should be addressed: e-mail, mark.thomas@ncl.ac.uk.

(1) Chou, M.-S.; Chiou, J.-H. *J. Environ. Eng.* **1997**, 437.
(2) Hassler, J. W. *Activated Carbon*; Chemical Publishing Co.: New York, 1963.
(3) Goss, K. U.; Eisenreich, S. J., *Atmos. Environ.* **1997**, *31*, 2827.
(4) Bilinski, B.; Wojcik, W. *Mater. Chem. Phys.* **1992**, *30*, 209.
(5) El Nabarawy, T.; Mostafa, M. R.; Youssef, A. M. *Adsorpt. Sci. Technol.* **1997**, *15*, 59.
(6) Gregg, S. J.; Langford, J. F. *Trans. Faraday Soc.* **1969**, *65*, 1394.
(7) Rodriguez-Reinoso, F.; Linares-Solano, A. In *Chemistry and Physics of Carbon*; Thrower, P. A., Ed.; Marcel Dekker: New York, 1989; Vol. 21, p 1.
(8) Reid, C. R.; Thomas, K. M. *Langmuir* **1999**, *15*, 3206.
(9) Reid, C. R.; O'koye, I. P.; Thomas, K. M. *Langmuir* **1998**, *14*, 2415.
(10) Harding, A. W.; Foley, N. J.; Norman, P. R.; Francis, D. C.; Thomas, K. M. *Langmuir* **1998**, *14*, 3858.
(11) Foley, N. J.; Forshaw, P. L.; Thomas, K. M.; Stanton, D.; Norman, P. R. *Langmuir* **1997**, *13*, 2083.

10.1021/la9814992 CCC: $15.00
Published on Web 08/05/1999

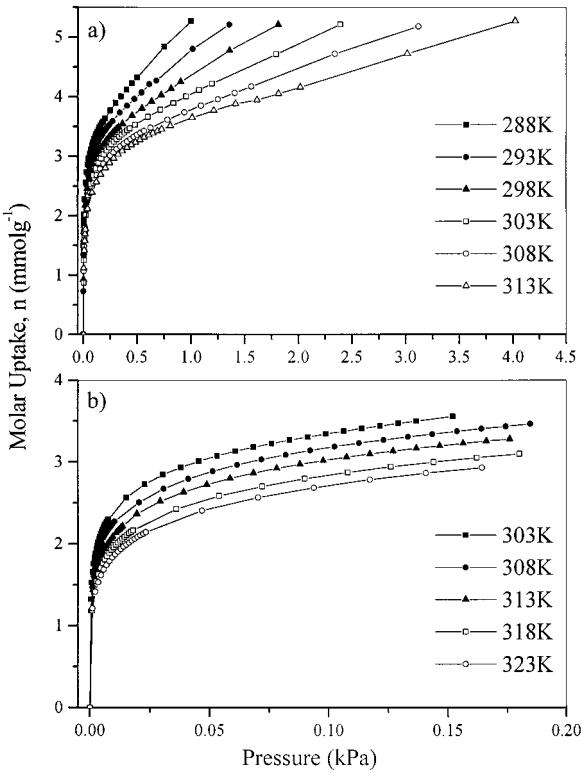

Figure 1. Adsorption isotherms for (a) *n*-octane and (b) *n*-nonane on BAX950.

and pressure control system were fully thermostated to 0.2 K to eliminate changes in the external environment. The microbalance had a long-term stability of ± 1 μg with a weighing resolution of 0.2 μg. The carbon sample (100 $\pm$ 1 mg) was outgassed until it reached a constant weight, at a pressure of $<10^{-6}$ Pa at 473 K. The liquid used to generate the vapor was degassed fully by repeated evacuation and vapor equilibration cycles of the liquid supply side of the vapor reservoir. The vapor pressure was gradually increased, over a time scale of ~30 s to prevent disruption of the microbalance, until the desired value was achieved. Pressure control was via the use of two pressure transducers with ranges 0 to 0.2 and 0−10 kPa, each with an accuracy of 0.02% of the specified range. The pressure was maintained at the set point by active computer control of the inlet/outlet valves throughout the duration of the experiment. Pressure steps in the range of p/p^o values 0−0.973 were used to obtain the isotherm. The mass uptake was measured as a function of time and the approach to equilibrium monitored in real time with a computer algorithm. After equilibrium was established, the vapor pressure was increased to the next set pressure value and the subsequent uptake was measured until equilibrium was reestablished. The increase in weight due to adsorbate uptake for each pressure step was used to calculate the kinetic parameters for adsorption. The errors in the calculated rate constants were typically better than 2% of the value. The sample temperature was constantly monitored throughout the duration of the experiment and the variation in temperature was minimal (<0.1 K). In the case of desorption the reverse procedure was carried out.

3. Results

3.1. Adsorption Isotherm Measurements. The adsorption isotherms for the adsorption of *n*-octane and *n*-nonane on BAX950 are shown in Figure 1. Both adsorption isotherms have a similar shape and do not fit into the IUPAC scheme very well because there is no well-defined plateau at high p/p^o as in a type I isotherm, which is the nearest to the overall shape. Similar behavior has been observed previously for *n*-octane adsorption on zeolites[13,14] and silicalite.[15] The data obtained for the various temperatures produced isotherms that showed excellent agreement on a relative pressure basis. Desorption of preadsorbed *n*-octane vapor from BAX950 was also investigated, and only very small amounts of hysteresis which increased with decreasing temperature were observed above an uptake of ~3.5 mmol g^{-1}.

3.2. Adsorption Kinetics. The kinetics of *n*-octane adsorption on BAX950 follow a linear driving force (LDF) mass transfer model[8] up to p/p^o ~0.175

$$M_t/M_e = 1 - e^{-kt} \tag{1}$$

where M_t is the uptake at time t, M_e is the equilibrium uptake, and k is the rate constant; hence a plot of $\ln(1 - M_t/M_e)$ versus time will be linear with a gradient equal to the rate constant.

Parts a and b of Figure 2 show typical plots of uptake versus time and the corresponding fits for the LDF model. Each graph represents a region of the isotherm which obeys the LDF model, to prove the model holds in the pressure range p/p^o ~0−0.175. The adsorption uptakes versus time graphs obey the LDF model for >90% of the total uptake for each specific pressure step, and the kinetic data are given in Table 1. Figure 2c shows an uptake curve and corresponding fit for the combined barrier/resistance model[16] for pressure step (p/p^o 0.4864−0.7296). This model is based on the existence of a barrier resistance at the surface and subsequent diffusion into a spherical particle governed by Fick's law. The equations for isothermal diffusion into a spherical particle are

$$\frac{\partial C}{\partial t} = D\left(\frac{\partial^2}{\partial r^2}\right) + \left(\frac{2}{r}\right)\left(\frac{\partial C}{\partial r}\right) \tag{2}$$

where D is the crystallite diffusivity ($cm^2\ s^{-1}$), C is the sorbate concentration in the crystallite (mmol cm^{-3}), r is the radial coordinate, and t is the time and

$$D\,\frac{\partial C(r_c t)}{\partial r} = k_b\{C^*(t) - C(r,t)\} \tag{3}$$

where k_b is the barrier resistance ($cm\ s^{-1}$), r_c is the radius of the particle (cm), and C^* is the surface concentration in equilibrium with the gas phase (mmol cm^{-3}). The parameters derived from the model are k_b, the barrier resistance constant, and k_d which is equal to D/r_c^2. The equations were solved by numerical methods.[8,9] The combined barrier resistance model fit is shown for the $\ln(1 - M_t/M_e)$ versus time graph which shows the deviation from the linearity observed for the linear driving force model. The adsorption kinetic data at pressures above p/p^o ~0.175 fit a combined barrier resistance/diffusion model, and this shows the change in the importance of diffusion relative to the barrier resistance in determining the overall adsorption dynamics.

Figure 3 shows the variation of *n*-octane vapor adsorption rate constants obtained from the LDF model with surface coverage for p/p^o 0−0.175. The rate constants for

(12) Benham, M. J.; Ross, D. K. *Z. Phys. Chem.* **1989**, *163*, 25.

(13) Houzvicka, J.; Klik, R.; Kubelkova, L.; Ponec, V. *Catal. Lett.* **1997**, *43*, 7.

(14) Vavlitis, A. P.; Ruthven, D. M.; Loughlin, K. F. *J. Colloid Interface Sci.* **1981**, *84*, 526.

(15) Sun, M. S.; Talu, O.; Shah, B. D. *J. Phys. Chem.* **1996**, *100*, 17276.

(16) Loughlin, K. F.; Hassan, M. M.; Fatehi, A. H.; Zahur, M. *Gas Sep. Purif.* **1993**, *7*, 264.

Table 1. Rate Constants for the Adsorption of *n*-Octane on Active Carbon BAX950 Obtained from the LDF Model

	$k/(s^{-1}) \times 10^4$					
p/p^o	288 K	293 K	298 K	303 K	308 K	313 K
0−0.00973	4.01 ± 0.23	5.97 ± 1.64	4.91 ± 1.39	10.8 ± 2.41	6.81 ± 0.92	11.8 ± 1.37
0.00973−0.00195	10.1 ± 0.64	8.93 ± 0.81	12.5 ± 0.72	15.6 ± 0.91	21.4 ± 0.68	26.8 ± 0.54
0.00195−0.00292	14.6 ± 1.35	15.9 ± 0.71	20.3 ± 0.67	22.6 ± 0.70	32.3 ± 0.74	40.0 ± 0.76
0.00292−0.00389	17.2 ± 0.83	21.1 ± 0.84	26.0 ± 0.81	28.9 ± 0.84	39.9 ± 0.88	48.1 ± 0.96
0.00389−0.00486	20.1 ± 0.76	25.1 ± 0.93	30.7 ± 0.86	32.3 ± 0.84	44.8 ± 1.03	55.3 ± 1.11
0.00486−0.00973	31.1 ± 0.37	38.3 ± 0.50	44.6 ± 0.62	49.3 ± 0.44	60.9 ± 0.61	69.1 ± 0.62
0.00973−0.01946	38.0 ± 0.46	45.9 ± 0.55	55.5 ± 0.72	67.4 ± 0.88	73.7 ± 0.96	84.5 ± 0.76
0.01946−0.02919	47.6 ± 0.57	57.9 ± 0.69	65.2 ± 0.98	74.5 ± 0.67	93.5 ± 1.31	100.9 ± 1.11
0.02919−0.03891	55.9 ± 0.67	72.3 ± 0.80	79.1 ± 1.11	85.0 ± 0.94	102.6 ± 1.23	123.6 ± 1.11
0.03891−0.04864	62.7 ± 0.75	79.1 ± 0.87	85.1 ± 1.28	96.1 ± 1.06	110.5 ± 1.55	115.5 ± 2.19
0.04864−0.05837	66.9 ± 0.80	90.7 ± 1.45	93.6 ± 1.31	113.5 ± 1.36	153.4 ± 2.45	167.8 ± 3.02
0.05837−0.06810	73.5 ± 0.88	98.7 ± 1.09	111.4 ± 1.56	133.0 ± 1.73	161.3 ± 2.90	183.8 ± 3.13
0.06810−0.07783	79.0 ± 0.87	107.1 ± 1.71	123.8 ± 1.86	152.7 ± 1.53	178.3 ± 2.14	223.7 ± 2.68
0.07783−0.08756	83.6 ± 0.84	114.3 ± 1.60	131.4 ± 1.45	160.8 ± 1.45	199.6 ± 2.00	235.3 ± 2.35
0.08756−0.09729	110.6 ± 1.55	123.8 ± 2.10	158.7 ± 2.06	181.8 ± 2.18	226.2 ± 2.94	229.9 ± 2.76
0.09729−0.10732	132.6 ± 1.46	146.0 ± 2.48	176.1 ± 1.94	189.0 ± 2.08	214.1 ± 3.00	246.9 ± 2.96
0.10732−0.11674	118.3 ± 0.95	152.2 ± 2.89	192.7 ± 2.31	196.5 ± 2.16	241.5 ± 2.17	268.8 ± 2.42
0.11674−0.12647	152.9 ± 1.68	175.4 ± 3.16	212.8 ± 1.70	248.8 ± 2.74	280.9 ± 2.81	276.2 ± 2.49
0.12647−0.1362	137.2 ± 1.10	197.2 ± 2.17	223.2 ± 1.79	253.2 ± 3.04	277.8 ± 1.94	282.5 ± 1.69
0.1362−0.14593	177.3 ± 2.13	224.7 ± 1.12	245.1 ± 2.45	286.5 ± 2.58	317.5 ± 1.27	357.1 ± 2.14
0.14593−0.15566	195.7 ± 3.33	248.8 ± 1.74	263.9 ± 1.58	300.3 ± 2.70	337.8 ± 1.69	353.4 ± 2.12
0.1556−0.16539	173.0 ± 3.11	239.8 ± 2.16	294.1 ± 2.06	310.6 ± 2.80	323.6 ± 2.27	384.6 ± 2.31
0.16539−0.17511	167.8 ± 2.52	251.3 ± 1.51	317.5 ± 2.22	306.7 ± 3.07	332.2 ± 2.33	383.1 ± 1.92

Table 2. Rate Constants for the Adsorption of *n*-Nonane on Active Carbon BAX950 Obtained from the LDF Model

	$k/(s^{-1}) \times 10^{-4}$				
p/p^o	303 K	308 K	313 K	318 K	323 K
0−0.00049	3.4 ± 0.01	3.7 ± 0.01	4.4 ± 0.01	6.0 ± 0.02	7.6 ± 0.03
0.00049−0.00097	10.5 ± 0.02	11.2 ± 0.03	12.9 ± 0.01	17.1 ± 0.08	20.4 ± 0.11
0.00097−0.00146	15.2 ± 0.06	17.1 ± 0.08	19.3 ± 0.01	23.3 ± 0.16	27.8 ± 0.19
0.00146−0.00195	18.8 ± 0.09	19.7 ± 0.13	22.6 ± 0.02	29.5 ± 0.25	32.9 ± 0.26
0.00195−0.00243	20.8 ± 0.11	24.2 ± 0.16	26.0 ± 0.25	32.2 ± 0.28	36.2 ± 0.33
0.00243−0.00292	23.7 ± 0.19	26.3 ± 0.21	30.6 ± 0.03	35.4 ± 0.41	42.1 ± 0.41
0.00292−0.00341	23.9 ± 0.24	26.9 ± 0.22	31.5 ± 0.03	39.2 ± 0.44	46.3 ± 0.49
0.00341−0.00389	27.0 ± 0.25	30.5 ± 0.26	37.7 ± 0.03	44.0 ± 0.52	50.4 ± 0.61
0.00389−0.00438	29.6 ± 0.37	32.1 ± 0.34	38.2 ± 0.02	48.9 ± 0.65	54.3 ± 0.68
0.00438−0.00486	29.1 ± 0.39	33.8 ± 0.43	41.8 ± 0.03	50.1 ± 0.65	59.5 ± 0.92
0.00486−0.00535	30.2 ± 0.33	37.7 ± 0.41	45.7 ± 0.03	52.4 ± 0.71	59.9 ± 0.86
0.00535−0.00584	34.4 ± 0.38	41.3 ± 0.53	47.3 ± 0.03	54.1 ± 0.70	57.7 ± 0.93
0.00584−0.00632	34.7 ± 0.43	41.9 ± 0.68	48.5 ± 0.03	56.2 ± 0.95	63.9 ± 1.14
0.006324−0.00681	36.5 ± 0.44	44.4 ± 0.59	48.6 ± 0.04	58.9 ± 0.90	69.3 ± 1.15
0.00681−0.00730	36.9 ± 0.49	43.3 ± 0.73	51.3 ± 0.05	59.5 ± 1.13	71.4 ± 1.27
0.00730−0.00778	39.9 ± 0.67	46.0 ± 0.93	53.4 ± 0.04	61.1 ± 1.12	72.2 ± 1.30
0.00778−0.00827	41.2 ± 0.73	47.8 ± 0.89	53.6 ± 0.86	61.5 ± 1.21	72.5 ± 1.37
0.00827−0.00876	42.7 ± 0.69	44.1 ± 0.86	54.3 ± 1.00	61.9 ± 1.34	74.7 ± 1.45
0.00876−0.00924	44.7 ± 0.69	51.2 ± 1.15	55.2 ± 1.10	63.8 ± 1.34	75.2 ± 1.53
0.00924−0.00973	46.4 ± 0.76	51.2 ± 1.07	55.5 ± 0.86	64.6 ± 1.25	77.3 ± 1.79
0.00973−0.01946	46.3 ± 0.34	51.5 ± 0.26	58.0 ± 0.24	66.4 ± 0.40	78.4 ± 1.72
0.01946−0.02919	47.6 ± 0.36	52.1 ± 0.33	60.0 ± 0.32	69.5 ± 0.53	81.6 ± 0.53
0.029189−0.03891	56.6 ± 0.51	59.8 ± 0.50	68.2 ± 0.56	81.6 ± 0.67	84.2 ± 0.78
0.03891−0.04864	64.1 ± 0.70	63.9 ± 0.65	73.6 ± 0.65	81.0 ± 0.85	88.8 ± 1.03
0.04864−0.05837	68.7 ± 0.85	70.9 ± 0.85	77.9 ± 0.73	92.0 ± 1.18	91.9 ± 1.18
0.05837−0.06810	76.4 ± 1.05	78.7 ± 0.99	89.0 ± 1.27	96.6 ± 1.40	114.7 ± 2.63

adsorption increase with increasing relative pressure and surface coverage.

The adsorption kinetics for *n*-nonane (see Table 2) are slower than those for *n*-octane and show similar trends following a linear driving force model in the p/p^o range 0−0.07, which corresponds to an uptake of ∼0−3 mmol g^{-1}. Above p/p^o ∼0.07, a combined barrier resistance/diffusion model provided a good fit to the adsorption kinetic data.

3.3. Desorption Kinetics. The kinetics of *n*-octane desorption from BAX950 follow a LDF mass transfer model in the pressure range p/p^o 0−0.175. Figure 4 shows the variations of *n*-octane vapor desorption rate constants with surface coverage compared to the rates for adsorption. The kinetic data for each pressure step for adsorption temperatures in the range 288−313K are given in Table 3. The rate constants for desorption are much slower in comparison with the corresponding rates for adsorption and decrease with decreasing relative pressure. The dramatic change in rate initially is due to the desorption of adsorbate from the meso- and macroporosity followed by the slower desorption from the microporosity.

4. Discussion

4.1. Adsorption Isotherms. The *n*-octane and *n*-nonane total pore volumes calculated from the uptake estimate for $p/p^o = 1$ were 0.85 and 0.89 $cm^3\ g^{-1}$, respectively. These pore volumes are similar to the corresponding pore volumes obtained from nitrogen adsorption at 77 K (0.83 $cm^3\ g^{-1}$) and water vapor adsorption (0.71 $cm^3\ g^{-1}$).[10] The lower pore volume obtained for the adsorption of water has been noted in previous studies[17−19] and can be ascribed to the lower density of

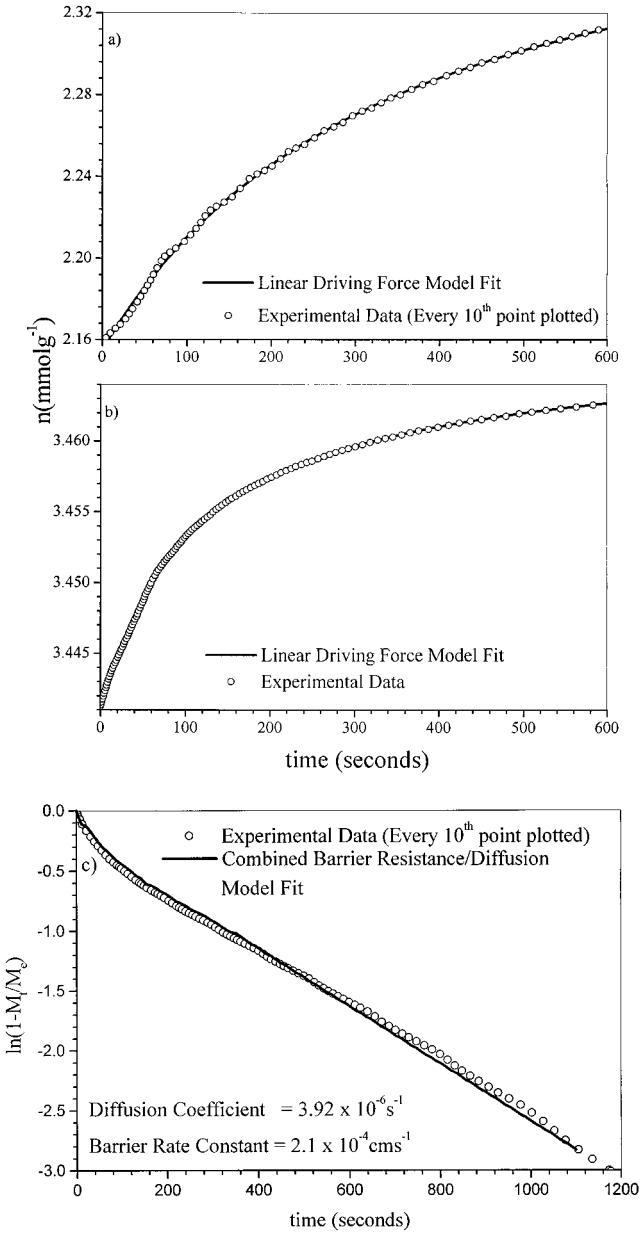

Figure 2. (a) Adsorption of *n*-octane on active carbon BAX950 at 288 K, $p/p^o = 0.00486-0.00973$ (5−10 Pa). (b) Adsorption of *n*-octane on active carbon BAX950 at 288 K, $p/p^o = 0.1167-0.1265$ (120−130 Pa). (c) Adsorption of *n*-octane on active carbon BAX950 at 288 K, $p/p^o = 0.4864-0.7296$ (500−750 Pa).

the adsorbed phase. Previous investigations have found that *n*-nonane molecules do not adsorb into the microporosity of some carbons.[20,21] The studies reported here for the adsorption of *n*-octane and *n*-nonane, on BAX950, show different behavior as indicated by the similar pore volume data for nitrogen (77 K), *n*-octane (288−313 K), and *n*-nonane (303−323 K) adsorption.

The micropore volume obtained from adsorption of carbon dioxide at 273 K was 0.18 $cm^3\ g^{-1}$ suggesting that BAX950 has an extensive meso- and macroporous structure in addition to a microporous structure.[10] The pore size distribution for BAX950 obtained from the nitrogen

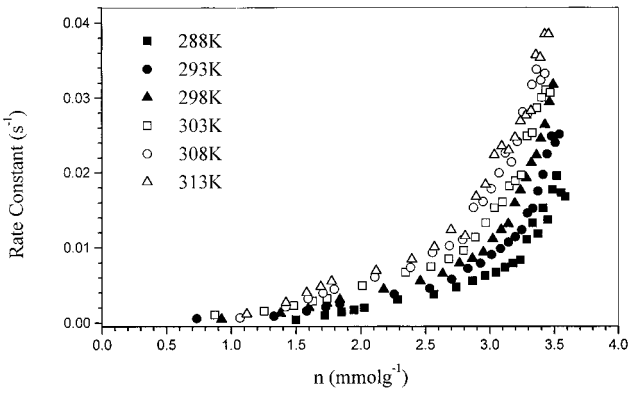

Figure 3. Variation of rate constant with amount of *n*-octane adsorbed (n/mmol g^{-1}) on active carbon BAX950.

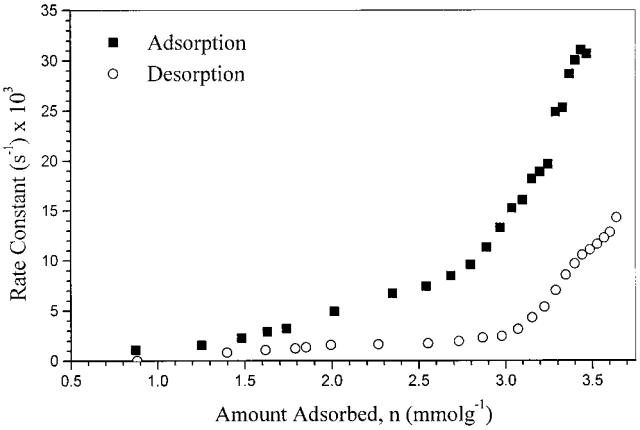

Figure 4. Variation of rate constant with amount adsorbed (n/mmol g^{-1}) for *n*-octane adsorption/desorption from active carbon BAX950 at 303 K.

(77 K) desorption isotherm by the method of Halsey[22] showed the presence of extensive mesoporosity as well as a significant amount of macroporosity.

The adsorption isotherms were compared using the Dubinin−Radushkevich (D−R) equation:

$$\log n = \log n_0 - B \log^2(p^o/p) \qquad (4)$$

where n is the amount adsorbed, n_0 the amount adsorbed corresponding to the micropore volume, p the pressure, p^o the saturated vapor pressure, and B a constant related to the microporous structure of the adsorbent. The D−R plots of the *n*-octane adsorption data were linear for the low-pressure region of the plot but deviated from linearity at higher pressures. The change between these two portions occurs at $p/p^o \sim 0.077$. This corresponds to a pore volume of ∼0.50 $cm^3\ g^{-1}$ which is intermediate between total pore volume (0.85 $cm^3\ g^{-1}$) and the micropore volume (0.18 $cm^3\ g^{-1}$). The deviation of the D−R graph from linearity indicates filling of available adsorption volume beyond that predicted by the micropore distribution function used in the D−R model.[23] The D−R plots for *n*-nonane adsorption gave less well-defined deviations from linearity at ∼2 mmol g^{-1} uptake corresponding to a volume of ∼0.36 $cm^3\ g^{-1}$.

4.2. Isosteric Enthalpies of Adsorption Using the Van't Hoff Isochore. The hysteresis for the *n*-octane adsorption isotherms was very small. Therefore, the isosteric enthalpies of adsorption were calculated using

(17) Bradley, R. H.; Rand, B. *Carbon* **1991**, *29*, 1165.
(18) O'Koye, I. P.; Benham, M.; Thomas, K. M. *Langmuir* **1997**, *13*, 4054.
(19) Rodriguez-Reinoso, F. *Carbon* **1998**, *36*, 159.
(20) Gregg, S. J.; Tayyab, M. *J. Chem. Soc., Faraday Trans. 1*, **1978**, *74*, 348.
(21) Hanzawa, Y.; Suzuki, T.; Kaneko, K. *Langmuir* **1994**, *10*, 2857.
(22) Halsey, G. D. *J. Chem. Phys.* **1948**, *16*, 931.
(23) Marsh, H. *Carbon* **1987**, *25*, 49.

Table 3. Rate Constants (k) for the Desorption of *n*-Octane from Active Carbon BAX950 Obtained from the LDF Model

	$k/(s^{-1}) \times 10^5$					
p/p^o	288 K	293 K	298 K	303 K	308 K	313 K
0.17511−0.16539	1047.1 ± 25.22	1209.2 ± 36.55	1353.2 ± 47.61	1430.6 ± 40.93	1686.3 ± 76.78	1915.7 ± 62.39
0.16539−0.15566	983.3 ± 14.50	1056.0 ± 21.19	1245.3 ± 43.42	1283.7 ± 29.66	1526.7 ± 74.59	1663.9 ± 27.69
0.15566−0.14593	925.9 ± 35.13	966.2 ± 19.60	1149.4 ± 39.64	1227.0 ± 36.13	1436.8 ± 43.35	1483.7 ± 26.42
0.14593−0.13620	881.1 ± 34.16	925.1 ± 15.40	1001.0 ± 25.05	1162.8 ± 41.91	1283.7 ± 37.90	1396.6 ± 37.06
0.13620−0.12647	715.8 ± 16.40	856.2 ± 14.66	927.6 ± 11.19	1108.6 ± 36.87	1248.4 ± 34.29	1287.0 ± 26.50
0.12647−0.11674	603.5 ± 20.03	757.0 ± 13.75	906.6 ± 7.40	1057.1 ± 34.64	1142.9 ± 30.04	1212.1 ± 29.38
0.11674−0.10701	561.5 ± 41.30	704.2 ± 6.94	792.4 ± 8.16	968.1 ± 29.99	1033.1 ± 27.75	1096.5 ± 19.24
0.10701−0.09729	473.9 ± 9.43	639.0 ± 6.53	685.4 ± 6.11	858.4 ± 23.58	888.9 ± 20.54	966.2 ± 14.94
0.09729−0.08756	420.3 ± 6.54	558.3 ± 4.99	623.1 ± 5.43	703.7 ± 15.35	780.0 ± 18.86	852.5 ± 12.36
0.08756−0.07783	360.4 ± 5.84	436.1 ± 4.56	524.4 ± 3.85	538.2 ± 10.43	639.8 ± 9.41	723.6 ± 11.52
0.07783−0.06810	280.3 ± 3.77	334.7 ± 3.92	367.6 ± 2.03	433.1 ± 7.88	503.8 ± 5.84	572.1 ± 6.22
0.06810−0.05837	214.4 ± 2.57	227.6 ± 1.55	266.0 ± 1.20	317.6 ± 4.24	380.0 ± 3.47	404.9 ± 2.95
0.05837−0.04864	203.1 ± 2.64	212.5 ± 2.03	228.2 ± 1.35	245.9 ± 4.78	282.6 ± 5.11	319.5 ± 1.74
0.04864−0.03891	175.7 ± 1.76	191.1 ± 2.34	202.5 ± 1.60	231.3 ± 4.65	239.6 ± 5.34	265.1 ± 1.19
0.03891−0.02919	158.7 ± 0.34	171.8 ± 2.36	180.1 ± 1.07	195.8 ± 6.90	204.5 ± 7.15	228.0 ± 1.77
0.02919−0.01946	140.9 ± 1.67	154.7 ± 1.96	163.3 ± 0.99	173.2 ± 2.07	196.1 ± 1.88	240.8 ± 1.86
0.01946−0.00973	129.1 ± 0.88	142.3 ± 1.20	146.7 ± 0.86	165.0 ± 6.81	177.4 ± 1.76	210.9 ± 1.56
0.00973−0.00486	116.2 ± 0.34	132.9 ± 1.94	135.9 ± 0.65	158.7 ± 2.69	177.3 ± 1.01	185.4 ± 1.31
0.00486−0.00389	115.8 ± 0.35	125.8 ± 0.98	124.6 ± 0.50	136.2 ± 2.22	163.2 ± 3.17	177.1 ± 1.29
0.00389−0.00292	100.8 ± 0.24	115.5 ± 0.84	119.2 ± 0.48	123.5 ± 2.90	147.2 ± 1.86	150.3 ± 1.76
0.00292−0.00195	100.4 ± 0.30	108.6 ± 1.78	118.8 ± 0.59	109.8 ± 1.99	143.7 ± 1.01	150.1 ± 2.01
0.00195−0.00097	6.5 ± 0.10	18.7 ± 0.65	86.9 ± 0.84	84.3 ± 1.12	125.1 ± 1.10	125.6 ± 0.68
0.00097−0	6.2 ± 0.05	2.4 ± 0.01	1.17 ± 0.002	1.47 ± 0.01	1.21 ± 2.10	1.83 ± 0.001

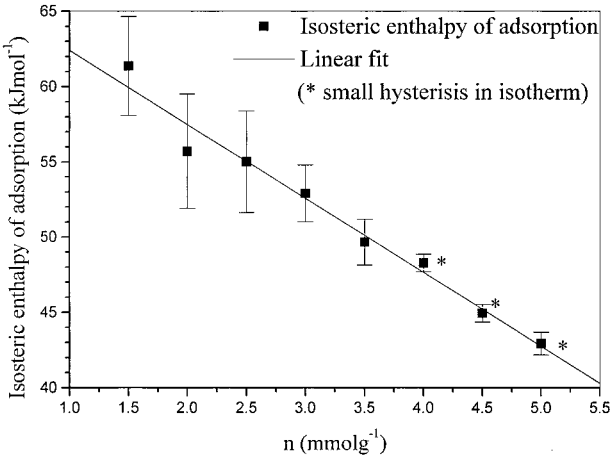

Figure 5. Isosteric enthalpies for *n*-octane adsorption on active carbon BAX950.

the van't Hoff isochore and the region where the isotherm exhibited a slight hysteresis is marked in Figure 5. The isosteric heats of adsorption decreased approximately linearly with increasing surface coverage. This is different from the usual fairly rapid decrease with increasing surface coverage followed by a plateau. The values obtained were in the range 43−61.5 kJ mol^{-1}, with a limiting isosteric enthalpy of 68 kJ mol^{-1} at zero surface coverage. This compares with the enthalpy of vaporization of 38.6 kJ mol^{-1} [24] and an approximate value of the heat of adsorption measured at low surface coverage by gas chromatographic methods for adsorption on graphitized thermal carbon black of ∼56 kJ mol^{-1}.[24] The *n*-nonane adsorption gives a similar trend in isosteric heats of adsorption with surface coverage and values in the range 57−68 kJ mol^{-1}. The corresponding values of the heat of vaporization[24] and low surface coverage heat of adsorption[25] for *n*-nonane are 43.8 and ∼62 kJ mol^{-1}, respectively.

4.3. Adsorption Kinetics. There are limited kinetic data available in the literature concerning the adsorption of gases and vapors on activated carbons due to the complexity of the experimental techniques involved and the difficulty in carrying out measurements at low pressures (<0.1 kPa). Rao et al. have developed a model[26] for the interaction potential of species diffusing in pores based on the previous model of Steele[27] for the interaction of gases with carbon surfaces. They concluded that two barriers existed: (a) entry into the pore and (b) diffusion along the pore. The rate-limiting process in carbon molecular sieves was entry into the pores, and in this case the overall adsorption kinetics follow a linear driving force model.[8,9] Nitrogen and oxygen adsorption on CMS materials are examples of adsorption kinetics which follow the LDF model and show differences in rate of ∼×25. Recent studies of the adsorption kinetics of carbon dioxide on the same CMS material have shown that the adsorption kinetic model may change from LDF through a combined barrier resistance/diffusion model to a Fickian diffusion with increasing pressure.[8] This was ascribed to the increasing importance of diffusion along the pores with increasing pressure, which becomes the rate-determining step at high pressure. At low pressure, diffusion through the barrier at the pore entrance was the rate-determining step. These studies refer to the diffusion of small molecules into a microporous material where the kinetic selectivity was introduced by carbon deposition. It was concluded that while the size of the adsorptive relative to the pore dimension was a factor, it was not the only factor and specific adsorbate−adsorbent interactions had a significant role in determining adsorption kinetics in these systems.

The adsorption of *n*-octane and *n*-nonane on active carbons have quite marked differences to the adsorption of small molecules on carbon molecular sieves in that the active carbon contains a much wider pore size distribution and the adsorptive is much larger in overall size and flexible so that the molecule can adopt many conformations to enter and diffuse through the porous structure. The dimensions of *n*-octane and *n*-nonane calculated using zero intermediate neglect of differential overlap (ZINDO) methods were 401.4 × 453.7 × 1283.3 pm and 401.4 × 452.4 × 1407.6 pm, respectively.[28] When considering

(24) *CRC: Handbook of Chemistry and Physics*, 71st ed.; CRC Press: Boca Ratan, FL, 1991.
(25) Avgul, N. N.; Kieselev, A. V. In *Chemistry and Physics of Carbon*; Walker, P. L., Jr., Ed.; Marcel Dekker: New York, 1970; p 1.
(26) Rao, M. B.; Jenkins, R. G.; Steele, W. A. *Langmuir* **1985**, *1*, 137.
(27) Steele, W. A. *Surf. Sci.* **1973**, *36*, 317.

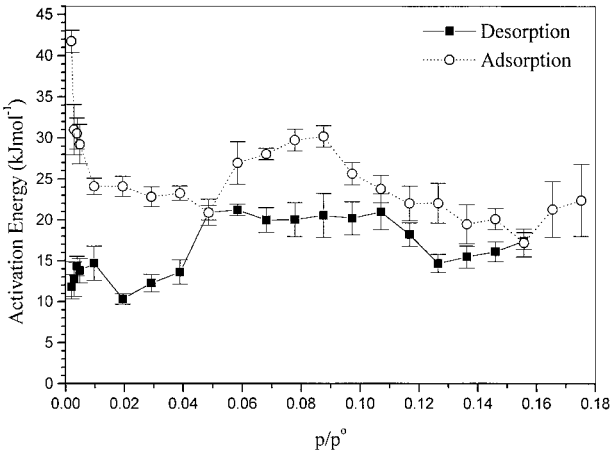

Figure 6. Comparison of activation energies for adsorption/desorption of *n*-octane on active carbon BAX950, temperature range 288−313 K.

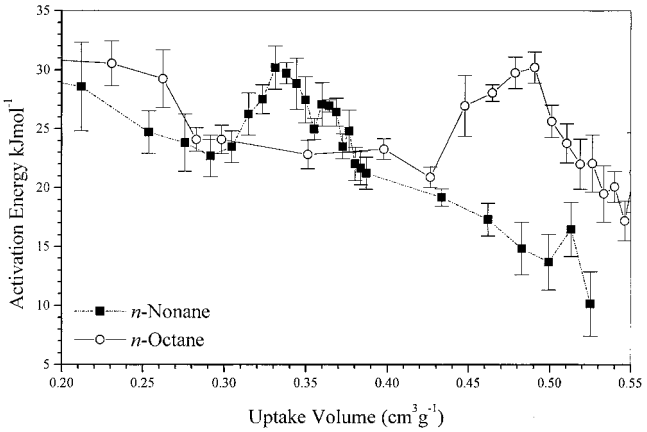

Figure 7. Comparison of activation energies for adsorption of *n*-octane and *n*-nonane on active carbon BAX950 on a volume uptake basis.

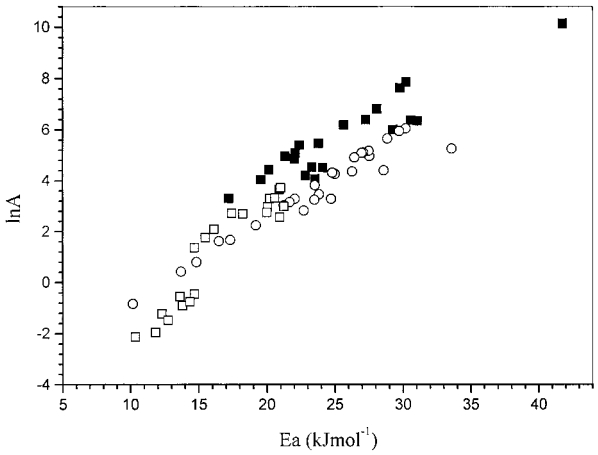

Figure 8. Variation of activation energy (E_a) with ln(preexponential factor) (ln(A)): adsorption of *n*-octane (■); adsorption of *n*-nonane (○); desorption of *n*-octane (□).

diffusion into spherical pores the two minimum dimensions need to be considered, whereas only the smallest dimension needs to be considered for diffusion into slit-shaped pores. As expected the two minimum dimensions for *n*-octane and *n*-nonane are virtually identical with differences only being observed in the third dimension (chain length). Therefore this factor is not a consideration in these studies. The kinetics for the adsorption of *n*-octane on BAX950 for the pressure range $p/p^o \sim 0-0.175$ follow a linear driving force mass transfer model while above $p/p^o \sim 0.175$ ($n \sim 3.5$ mmol g^{-1} or volume adsorbed ~ 0.56 cm^3 g^{-1}) a combined barrier resistance/diffusion model is followed, as shown in Figure 2c. The adsorption of *n*-nonane on the carbon shows similar trends with change from LDF to combined barrier resistance/diffusion model occurring at a $p/p^o \sim 0.07$ (amount adsorbed (n) ~ 3 mmol g^{-1} or volume adsorbed ~ 0.5 cm^3 g^{-1}). Therefore there are similarities in the kinetic laws observed for adsorption of small molecules on CMS and much larger molecules on active carbons. The rate constants in Table 1 correspond to the progressive stepwise adsorption of *n*-octane on BAX950 over a range of surface coverage and temperatures. The rate increases with relative pressure and surface coverage. The isosteric enthalpy of adsorption decreases, indicating that surface diffusion into the porous structure increases with increasing surface coverage.

To investigate the barriers to diffusion, the activation energies were calculated for the various relative pressure increments using the Arrhenius equation. The pressure increases were carried out in relative pressure terms so that the activation energies correspond to changes in specific surface coverage. Figure 6 shows the activation energy for adsorption of *n*-octane on BAX950. It is apparent from this graph that the highest values are obtained at the lowest p/p^o, while there is another maximum at $p/p^o \sim 0.075$ corresponding to an adsorption uptake ~ 0.48 cm^3 g^{-1}. The activation energies cover the range up to ~ 40 kJ mol^{-1}, and similar values have previously been obtained for water adsorption on BAX950.[10] There is an initially large value for the activation energy due to initial filling of the highest energy porosity (molecular sieving effect). A decrease in activation energy is then observed as the micropore volume is filled (up to $p/p^o = 0.005$), corresponding to a pore volume of ~ 0.22 cm^3 g^{-1}. This value is similar to the micropore volume (0.18 cm^3 g^{-1}) obtained using carbon dioxide adsorption at 273 K.[10] A peak was observed at $p/p^o \sim 0.075$, which is associated with changes in the pore filling mechanism. This maximum occurs at a relative pressure, which corresponds, to the point at which a marked deviation from linearity is observed in the D−R plots for these data. Previous studies have shown that when the pore size distribution is wide containing supermicroporosity and mesoporosity and the filling of this porosity possibly causes the D−R plot curvature.[23] Hence it is possible to conclude that the activation energy maximum is related to this phenomenon, with the peak resulting from an increase in the diffusional barrier as cooperative effects in pore filling cause restricted access to porosity.

The adsorption of *n*-nonane on BAX950 shows similar kinetic behavior to *n*-octane. Comparison of the activation energy data for *n*-octane is shown in Figure 7 on a volume of adsorbate basis. It is apparent that the peak in activation energy for *n*-nonane occurs at ~ 0.34 cm^3 g^{-1}, compared with ~ 0.48 cm^3 g^{-1} for *n*-octane. The peak in the activation energy is around 30 kJ mol^{-1} for both *n*-octane and *n*-nonane. The observation of the peak in the activation energy barrier at a lower uptake volume is consistent with the slower diffusion of *n*-nonane.

Figure 8 shows the variation of activation energy (E_a) with ln(A)(ln(preexponential factor)) obtained from the LDF model for both *n*-octane and *n*-nonane adsorption and *n*-octane desorption. The graphs are approximately parallel and it is apparent that there is a compensation effect. A similar compensation effect has been observed

(28) Webster, C. E.; Drago, R. S.; Zerner, M. C. *J. Am. Chem. Soc.* **1998**, *120*, 5509.

for the adsorption/desorption of water vapor on active carbons.[10] The mechanisms of adsorption of water vapor and hydrocarbons on active carbons are very different. The explanation of the compensation effect for adsorption/desorption kinetics in porous solids is consistent with a model, which includes two factors in the adsorption kinetics, (a) diffusion along the pores to the barrier and (b) diffusion through the barrier at the pore entrance. The LDF model is followed when the latter is the rate-determining step. Essentially a high activation energy barrier leads to buildup of adsorbate at the barrier giving a high preexponential factor and vice versa. Hence the activation energy and ln(preexponential factor) parameters are related. The diffusion of *n*-nonane is slower than *n*-octane, and this is reflected in the lower ln(*A*) values at a given activation energy.

A number of models for diffusion and adsorption in activated carbons have been developed based on surface diffusion, pore diffusion etc.[29−38] The driving force for surface diffusion is usually taken as the chemical potential gradient. These models use carbon structural parameters, for example, pores size distribution, and allow predictions of surface diffusivity versus surface coverage. These models predict a sharp increase in the surface diffusivity with increasing surface coverage, and an increase in the rate constant is observed for both *n*-octane and *n*-nonane in these studies. However, for surface coverages where pore filling was taking place, a decrease in diffusivity has been observed.[35] The results presented in this paper show that the kinetic rate constants observed for the adsorption of *n*-octane and *n*-nonane an BAX950 continue to increase into the pore filling region.

4.4. Desorption Kinetics. There is very limited literature concerning the desorption of gases and vapors on activated carbons again due to the complexity of the experimental techniques involved in measurements at low relative pressures, and at all pressures, data for desorption kinetics are extremely limited. The adsorption of *n*-nonane on active carbons has been studied extensively in connection with its use as a preadsorbent to fill the micropores while leaving the mesopores, macropores, and external surface free. Long-chain alkanes are difficult to remove from the micropores under vacuum.[6,7,39,40] The rate constants obtained for the desorption of octane provide support for the case for this particular system (see Figure 4). As the system pressure decreases, the rate of desorption becomes very small suggesting that there is difficulty in desorbing the long chain alkane from the micropores.

The activation energy barriers for desorption do not change dramatically and are typically in the range 10−22 kJ mol^{-1} for most of the isotherm. The activation energies as a function of surface coverage appear to follow the same trend as those obtained for adsorption. The compensation effect observed for the desorption Arrhenius parameters can be explained in a manner similar to the compensation effect for the adsorption parameters.

5. Conclusions

The adsorption kinetics of *n*-octane and *n*-nonane vapor follow a linear driving force mass-transfer rate law for >90% of the adsorption process for the pressure increments over the pressure range $p/p^o \sim 0-0.175$ for *n*-octane and 0−0.07 for *n*-nonane. A combined barrier resistance/diffusion model fits the adsorption kinetic data for pressure increments above these relative pressure ranges. Similar behavior has been observed for the diffusion of small molecules into carbon molecular sieves. The slowest rates are observed for adsorption at low relative pressures with a steady increase in rate with increasing relative pressure. The fastest adsorption rates correspond to the high p/p^o region. The desorption characteristics over the same pressure range also followed a linear driving force model for *n*-octane. The corresponding rate constants obtained for the desorption process show a reverse trend to adsorption, i.e., the rates are slowest at low relative pressures.

The activation energy for adsorption is at a maximum at the lowest relative pressures where diffusion into highest energy sites in the microporosity occurs and is, in effect, molecular sieving. Similar barriers in the 40−50 kJ mol^{-1} region have been observed for the diffusion of a wide range of adsorptives, for example, nitrogen into a carbon molecular sieve.[9,10] The activation energy of the adsorption process decreases with increasing adsorption until reaching a maximum at an uptake of 0.48 cm^3 g^{-1} for *n*-octane and ∼0.34 cm^3 g^{-1} for *n*-nonane. These barriers can be ascribed to the increased resistance to diffusion in the carbon due to cooperative effects in the pore-filling mechanism leading to restricted access to the porous structure. The compensation effect observed for adsorption of both *n*-octane and *n*-nonane and desorption of *n*-octane on the active carbon can be explained by a model involving two barriers (a) diffusion along the pores to the barrier and (b) diffusion through the barrier. The rate of transport of molecules through the barrier controls the concentration of molecules at the barrier. High activation energy restricts the transport of molecules through the barrier at the pore entrance leading to an increase in the preexponential factor obtained from the Arrhenius equation and vice versa.

Acknowledgment. The research was supported by an EPSRC studentship for A.J.F.

LA9814992

(29) Higashi, K.; Ito, H.; Oishi, J. *J. At. Energy Soc. Jpn.* **1963**, *5*, 846.
(30) Yang, R. T.; Fenn, J. B.; Haller, G. L., *AIChE J.* **1973**, *19*, 1052.
(31) Yang, R. T. *Gas Separation by Adsorption Processes*; Butterworths: Boston,
(32) Kapoor, A.; Yang, R. T.; Wong, C. *Catal. Rev. Sci. Eng.* **1989**, *31*, 129.
(33) Sladek, K. J.; Gilliland, E. R.; Baddour, R. F. *Ind. Eng. Chem. Fundam.* **1974**, *3*, 308.
(34) Tamon, H.; Okazaki, M.; Toei, R. *AIChE J.* **1981**, *27*, 271.
(35) Bhatia, S. K.; Do, D. D. *Proc. R. Soc.* **1991**, *434*, 317.
(36) Chen, Y. D.; Yang, R. T. *AIChE J.* **1991**, *37*, 1579.
(37) Chen, Y. D.; Yang, R. T. *Carbon* **1998**, *36*, 1525.
(38) Do, D. D.; Wang, K. *Carbon* **1998**, *36*, 1539.
(39) Gregg, S. J.; Sing, K. S. W. *Adsorption, Surface Area and Porosity*; 2nd ed.; Academic Press: London, 1982.
(40) Gregg, S. J.; Stock, R. *Trans. Faraday Soc.* **1957**, *53*, 1355.